Quantifying Dry Supercritical CO_2-Induced Changes of the Utica Shale

Sean Sanguinito[a,b]*, Angela Goodman[a,], Mary Tkach[a], Barbara Kutchko[a] Jeffrey Culp[a,b], Sittichai Natesakhawat[a,c], Jim Fazio[a,b], Isis Fukai[a,d] , Dustin Crandall[a]

[a]United States Department of Energy, National Energy Technology Laboratory, P.O. Box 10940, Pittsburgh, PA 15236

[b]AECOM Corporation, Pittsburgh, PA 15236

[c]Department of Chemical and Petroleum Engineering, University of Pittsburgh, Pittsburgh, PA 15261

[d]Presently at Battelle Memorial Institute, 505 King Ave. Columbus, OH 43201

To be submitted to: Fuel as a research paper

* Corresponding author. Tel.: 1-412-386-5434; Fax: 1-412-386-5870.

E-mail address: Sean.Sanguinito@netl.doe.gov

Abstract

Traditionally, shale formations have been studied as sealing layers that prevent vertical migration of hydrocarbons and CO_2 due to their low permeability and fracture porosity. Recent research has focused on storing CO_2 in hydrocarbon-bearing shale formations that have already undergone depletion through primary production and using CO_2 as a potential fracturing agent for unconventional reservoirs. The injected CO_2 will interact with shale components (i.e. clays, organic matter) and affect rock properties through chemical alteration, matrix swelling/shrinkage, and related geomechanical effects. As changes in rock properties will impact both anthropogenic CO_2 storage and hydraulic fracturing, it is imperative to increase our understanding of the CO_2-shale interactions. *In-situ* Fourier Transform infrared (FT-IR) spectroscopy coupled with high temperature and pressure capability was used to examine the interaction of dry CO_2 on Utica Shale, clay, and kerogen samples at the molecular scale and characterize vibrational changes of sorption bands sensitive to the gas-solid environment. The Utica Shale was also analyzed for micro and macro-scale chemical and physical changes before and after exposure to dry CO_2 at subsurface storage conditions using surface relocation techniques via high-resolution field-emission scanning electron microscopy (FE-SEM). Brunauer-Emmett-Teller (BET) surface area/pore size analysis and quantitative adsorption isotherms were applied to understand changes in surface area, pore volumes, and understand the storage potential of CO_2 in the Utica Shale sample. FT-IR and feature relocation via FE-SEM indicate carbonate formation and dissolution occurs in shale exposed to dry CO_2. Results indicate that etching and pitting occur, with minor calcite precipitation along the surface of the shale sample. Quantitative isotherm results indicate that shales with a higher content of kerogen and illite-smectite clays would be expected to have the highest CO_2 storage capacity provided these constituents were accessible for interaction.

Key words (4-6): CO_2 storage; shale; carbonate; dissolution; etching

1. Introduction

As climate change becomes an increasingly critical environmental issue, efforts are being made to reduce or divert anthropogenic CO_2 emissions from the atmosphere with Geologic Carbon Sequestration (GCS). GCS is a process where anthropogenic CO_2 that has been captured, typically at the source where it is generated (e.g. fossil-fuel burning power plant), is injected and stored in the subsurface within various geologic formations such as saline formations, depleted oil and gas reservoirs, unmineable coal seams, basalts, and shale formations (Orr, F.M., 2009a.; Orr, F.M., 2009b; US-DOE-NETL, 2015). Additionally, CO_2 is being used as an agent to enhance oil recovery from conventional reservoirs and as a potential fracturing agent for unconventional reservoirs, where a portion of the CO_2 is stored in the subsurface as a result of these activities (Jacobs, 2014; Xue et al., 2016).

Due to the growth in shale hydrocarbon exploration, GCS in depleted shale formations is gaining interest (Orr, F.M., 2009a; Orr, F.M., 2009b; Romanov et al., 2015; Levine et al., 2016). Only hydrocarbon-bearing shale formations that have already undergone depletion through primary production, or are planned to be produced in the future, are considered as potential geologic sinks for CO_2. Levine et al., (2016) listed the following criteria required for CO_2 storage in shales: (1) hydrocarbon production using horizontal drilling and stimulation via staged, high-volume hydraulic fracturing must occur prior to GCS operations, (2) CO_2 must be injected at depths sufficient to maintain CO_2 in a supercritical state (generally greater than 800 m), and (3) a seal must be present overlying the shale formation targeted for GCS. Storage of CO_2 in shale is expected to occur as a free phase within hydraulic and natural fractures and matrix pores and as a sorbed phase on organic and inorganic matter such as kerogen and clays. CO_2 has the potential to be utilized as a hydraulic fracturing fluid to reduce water use, increase hydrocarbon production, and create greater access to pore space (Jacobs, 2014; Xue et al., 2016). Thus, understanding CO_2 interactions with shale provides insight into issues facing CO_2 storage and hydraulic fracturing activities. It is important to note that most unstimulated shales serve as reservoir seals for hydrocarbon reservoirs and for GCS. This means these reactions between CO_2 and shale will commonly occur at the interface between a storage formation and the overlying seal. The nature of these reactions will have implications related to possible leakage and long term storage potential.

The majority of research has focused on CH_4 sorption on the organic component in shales (Ross and Bustin, 2007, 2008, 2009; Loucks et al., 2009; Zhang et al., 2012) with some work on CH_4 and CO_2 interactions on various clay components such as montmorillonite, kaolinite, and illite (Liu et al., 2013; Rother et al., 2013; Krukowski et al., 2015; Roychaudhuri et al., 2013; Wang et al., 2015). Ross and Bustin (2009) examined controls for CH_4 in a suite of Jurassic and Devonian-Mississippian shales from western Canada in terms of organic content, inorganic components, and thermal maturity. They found that both organic and clay minerals such as illite were important for controlling CH_4 storage capacity. In general, reports on high-pressure CO_2 sorption isotherms on shales are sparse (Romanov et al., 2015). Busch et al. (2008) examined the CO_2 sorption potential of a Muderong shale sample from Australia and its clay components – Ca-rich montmorillonite, Na-rich montmorillonite, illite, and kaolinite – at subsurface conditions relevant to storage. They found evidence for significant storage potential in shales that included physical sorption of CO_2 on clay minerals as well as CO_2 dissolution and geochemical reactions. Lahann et al. (2013) examined the influence of CO_2 on the New Albany shale with high and low organic contents and high carbonate content and observed dissolution of carbonate-mineralized biogenic structures. Bacon et al. (2015) provided the first field-scale modeling effort of CH_4 production and CO_2 injection to include both organic and clay sorption behavior in shale gas production models to improve accuracy. They found that the CO_2 sorption potential was similar for both organic matter and montmorillonite clay.

The objective of this work is to investigate the interaction of CO_2 with shale and identify and quantify chemical and physical alterations at the molecular and micro-scale. The shale being investigated is the Utica Shale first described by Emmons (1842) and chosen for this study because the formation is being targeted for hydrocarbon production and it represents a potential reservoir for CO_2 storage. Specifically, this study focuses on characterizing the surface interactions of the interface between CO_2 and the Utica Shale with *in-situ* Fourier Transform infrared spectroscopy (FT-IR), feature relocation scanning electron microscopy (SEM), Brunauer-Emmett-Teller (BET) surface area and pore size analysis, and quantitative adsorption isotherms at pressure and temperature conditions relevant for geological storage. We also examine surface interactions of primary individual constituents of the Utica Shale such as clays [illite-smectite, illite, chlorite, and

kaolinite] and kerogen to further investigate the mechanism responsible for reactions at the CO_2-shale interface.

2. Materials and experimental methods

2.1. Utica Shale: Flat Creek Member (US-1)

The Utica Shale is a calcareous, organic-rich shale deposited in the Appalachian Basin during the Middle Ordovician Taconic Orogeny (Smith and Leone, 2010). The typical depth for shale gas in the Utica ranges from 700-1800 m with an average net thickness of 150 m (Smith and Leone, 2010; Jarvie, 2012). The Utica Shale (US-1) was collected in the state of New York from an outcrop of the Utica Shale Flat Creek Member (Table 1) and is considered over-mature (Hulver, 1997; Rowan, 2006). Samples were collected from the interior of the outcrop to reduce weathering affects. The shale sample was stored in a nitrogen desiccator prior to characterization.

2.2. Clay samples

Clay samples - illite-smectite (ISCz-1), illite (IMt-2), chlorite (CCa-2), and kaolinite (KGa-1b) - were selected based on clays that were representative of the US-1 shale sample (Table 2). These clay standards were purchased from the Clay Mineral Society and used as received. Chlorite (10-20%), illite (55-70%), illite-smectite (15-25%), illite-chorite (trace), and kaolinite (trace) are common clays found in the Middle and Upper Devonian shale units in the Appalachian basin (Bacon et al., 2015; Hosterman and Whitlow, 1983). Qualitative X-Ray Diffraction (XRD) analysis of the US-1 shown in Table 3 supports the findings in the literature. Smectite clays are not common in thermally mature shales as with increased burial depth and temperature; smectite is converted into illite via mixed layer illite/smectite formation. This process is known as smectite diagenesis or smectite illitization (Pollastro, 1993). These samples represent a wide spectrum of clay mineral structures such as 1:1 repeating tetrahedral-octahedral (TO) layers (kaolinite), 2:1 alternating TOT layers (illite), mixed-layer (illite-smectite), and 2:1 +1 alternating TOT layers (chlorite).

2.3. Kerogen

A kerogen sample (NAk-1) was analyzed to study the effects of organic matter which is prevalent in shale. Due to limited sample quantity of the Utica Shale, we were unable to extract

enough kerogen for the sample characterization and measurements needed in this study. As a proxy for kerogen found in the Utica Shale, kerogen extracted from the New Albany Shale was provided by Maria Mastalerz at the Indiana Geological Survey. This kerogen (NAk-1) still contained some clay/quartz material as it is very difficult to extract pure kerogen from shale.

Table 1. Utica Shale sample information

Geologic Background

Basin	*Description*		*Sample Location*	
			Latitude	*Longitude*
Appalachian	Utica Shale: Flat Creek Member	Stream Bed Outcrop	42° 53' 11" N	74° 33' 53" W

Table 2. Clay and kerogen sample information

Sample ID	*Type*
KGa-1b	Kaolinite
IMt-2	Illite
ISCz-1	Illite-Smectite
CCa-2	Chlorite
NAk-1	Kerogen extracted from the New Albany Shale

Table 3. XRD analysis

Sample	*Quartz*	*Clay*	*Calcite*	*Dolomite*	*Albite*	*Chlorite*	*Pyrite*
US-1	minor	major	major	trace	minor	-	trace
Major > 25%			Minor: 5-25%			Trace < 5%	

*Mineral amounts are not quantitative and error is not known.

2.4. Total organic carbon

Carbon analysis for the shale sample was performed using a UIC incorporated CM014 carbon dioxide coulometer integrated with a CM5130 acidification module and a CM5300 combustion furnace apparatus. The working range for the UIC unit is from less than one microgram of carbon (μg C) up to 10,000 micrograms of carbon for a single sample and an optimal carbon

concentration range between 1000-3000 μg C. Total inorganic carbon (TIC), carbon derived from mineral weathering, was determined using acidification followed by electrochemical titration of the released CO_2 in the coulometer detector cell. Total carbon (TC) was determined by burning the sample at 935 °C in pure oxygen in the combustion furnace apparatus followed by electrochemical titration of the released CO_2 in the coulometer detector cell. Five replicates were conducted for the shale sample. Total organic carbon (TOC) was calculated by subtracting the average TIC value for each sample from its average TC value.

2.5. Attenuated Total Reflectance-FT-IR spectroscopy

Attenuated Total Reflectance-Fourier Transform Infrared Spectroscopy (ATR-FT-IR) measurements were collected with a single-beam (Thermo Electron Nexus 4700 FT-IR ESP) spectrometer equipped with a liquid nitrogen cooled wide-band MCT detector that allows for spectral collection from 4000 to 600 cm^{-1}. Each recorded spectrum was averaged from 250 scans with an instrument resolution of 2 cm^{-1}. High pressure and temperature experiments were conducted in custom-designed Spectra Tech ATR cells. See Goodman et al. (2005) for more details on the ATR cells. A syringe pump (ISCO 260D) was used to introduce gases to the ATR cells and regulate pressure conditions while a recirculating water bath used a 50:50 ratio of water to ethylene glycerol to regulate temperature.

All geologic samples: Utica Shale (US-1), illite-smectite (ISCz-1), illite (IMt-2), chlorite (CCa-2), kaolinite (KGa-1b), and kerogen (NAk-1) were powdered by mortar and pestle and sieved to 50 microns. An aliquot of powdered sample was then mixed with Millipore water to form a slurry and a small amount of slurry (~10 mg) was painted onto the sample ZnSe ATR crystal in a thin even coating. The blank ZnSe crystal was left uncoated. The sample (coated) and blank (non-coated) crystals were placed inside the ATR cells and sealed with Teflon O-rings to provide a high-pressure seal. The high-pressure ATR cells were loaded inside the FT-IR spectrometer on a linear translator stage capable of moving each cell into the IR beam path for data collection without disrupting experimental conditions.

The temperature was set to 40 °C and spectral scans were recorded of the blank and sample cells. These scans were used as a reference background and all subsequent scans were processed using them. Next CO_2 (99.998% supercritical grade) was introduced and the system was pressurized to 0.25 MPa. The blank and sample cells were scanned periodically until all changes

in the IR spectra stabilized (7-15 days). This process was repeated at increasing pressures of 0.5, 2.7, 5.5, and 8.2 MPa. At the end of the experiment, CO_2 was removed from the cells and the temperature was increased to 80 °C while N_2 was flowed gently through the cells to dry the sample and remove non-structural water. Samples were scanned periodically until the infrared water adsorption bands (ν_3 anti-symmetric stretching mode, ν_1 symmetric stretching mode, and ν_2 bending mode) between 3560 – 3000 cm^{-1} and 1630 cm^{-1} no longer changed with time. Finally, the temperature was reduced back to 40 °C, CO_2 was reintroduced, and stepwise increasing pressure scans were repeated for the dry samples.

2.6. Scanning Electron Microscopy

Intact, polished Utica Shale samples were analyzed prior to any exposure. Multiple sites were selected for imaging and feature relocation (Dieterich et al., 2016; Kutchko et al., 2013). After the initial SEM examination, the unexposed samples were placed inside 500 mL Teflon lined containers within autoclaves. The autoclaves were pressurized with dry supercritical CO_2 to simulate a reservoir pressure of 10.3 MPa and temperature of 40 °C and the samples were exposed to this environment for 14 days. These pressure and temperature conditions were chosen to represent acceptable storage conditions based on criteria laid out by Levine et al. (2016). Afterwards, the autoclaves were slowly depressurized over 5-6 hours to ensure sample integrity and the initial sites were relocated within the FE-SEM.

Characterization of the polished samples was conducted on a FEI Quanta 600 FEG environmental-scanning electron microscope equipped with energy dispersive X-ray Spectroscopy (EDS). All samples were examined in low vacuum mode without a conductive coating. Both backscattered electron (BSE) and secondary electron (SE) images were collected. SE imaging was used to reveal topography and morphology, while BSE and EDS analyses were used to distinguish phases within the shale samples. Brightness in a BSE image is proportional to the average atomic number of a given phase composition. EDS reveals the relative abundance of elemental data used to infer minerals present.

2.7. Brunauer-Emmett-Teller surface area and pore size analysis

Sorption isotherm measurements were conducted with unexposed and CO_2-exposed US-1 samples in a Quantachrome Autosorb 1-C surface area analyzer. Prior to analysis, the US-1 sample

was exposed to CO_2 in a reaction vessel at 40 °C and 10.3 MPa for 14 days. The sample (approximately 0.3 g) was subsequently degassed under vacuum at 110 °C for 4 hours to remove weakly-bound moisture. Adsorption-desorption isotherms of N_2 were conducted at -196 °C and the relative pressures (P/P_0) between 5 x 10^{-7} and 0.995. P_0 is the saturated vapor pressure of the adsorbate. In this work, P_0 is 0.101 MPa for N_2 at -196 °C and 3.485 MPa for CO_2 at 0 °C. Multipoint N_2-BET measurements were accomplished at the P/P_0 range of 0.1-0.3. CO_2 adsorption isotherm was also performed at 0 °C and P/P_0 between 1 x 10^{-6} and 0.03 to determine the volume and size distribution of ultra-micropores (i.e., pore diameter < 0.7 nm). Quenched solid and non-local density functional theory (QSDFT/NLDFT) methods were utilized for performing pore size analysis over the complete range of micro- and mesopores. The QSDFT (N_2-carbon-77K kernel) based on a slit/cylindrical pore model was applied on the adsorption branch of N_2 isotherms whereas the NLDFT (CO_2-carbon-273K kernel) model was applied on the CO_2 isotherms.

2.8. CO_2 adsorption isotherms

Gravimetric gas adsorption measurements for the NAk-1 and CCa-2 samples were obtained using a Hiden IGA microbalance (Warrington, England). Samples were not dried prior to measurement and only exposed to vacuum long enough to establish a zero pressure point at the start of the isotherms (15-30 minutes). Isotherms were measured under flowing gas regulated by a mass flow controller and back pressure regulator. Equilibrium was determined at each pressure step using an internal fitting algorithm in the instrument control software. Buoyance corrections were then applied to the final equilibrium weights using known densities of all components in the sample and counter weight chambers and gas densities calculated using REFPROP software (Lemmon et al., 2013). The densities of the samples (1.6823 g/cm^3 for NAk-1 and 2.7507 g/cm^3 for CCa-2) were determined prior to running the CO_2 isotherms using a helium pycnometer.

Isotherms were collected for US-1, illite, kaolinite, and the mixed layer illite-smectite on a pressure−composition isotherm measurement system (Advanced Materials Corp., Pittsburgh, PA) for pressures up to ∼1.5 MPa for CO_2. The instrument is designed on the basis of a conventional Sievert apparatus.

3. Results and discussion

3.1 Carbon analysis

Table 4 shows quantitative results for total carbon (TC), total inorganic carbon (TIC), and total organic carbon (TOC) for US-1. The total carbon content of the Utica Shale sample is 9.9 wt.% with the vast majority of carbon being inorganic.

Table 4. Carbon analysis results for the Utica Shale

Carbon Analysis Results

Total Carbon		*Total Inorganic Carbon*		*Total Organic Carbon*	
Carbon (%)	Std. Dev.	Carbon (%)	Std. Dev.	Carbon (%)	Std. Dev.
9.86	0.08	9.41	0.14	0.45	0.17

3.2. CO_2-Utica Shale interactions

As recent studies have indicated that CO_2 sorption in shales is correlated with organic content and sometimes clay content, our objectives were to examine the interaction of CO_2 with the Utica Shale, kerogen, and clay minerals and to examine any chemical or physical alteration of these materials upon CO_2 exposure. CO_2 may interact directly with shale fractures in regions of the formation where *in-situ* fluids and hydraulic fracturing fluids were displaced during injection (Pruess and Müller, 2009). Iwai et al. (2000) has shown that supercritical CO_2 can act as a drying agent to displace water by dissolving in the CO_2. Recent advances in *in-situ* analysis techniques such as spectroscopy, X-ray computed tomography, x-ray diffraction (XRD), and SEM can probe the interface of the CO_2-fluid-mineral reactions at subsurface storage temperature and pressure conditions (Lee et al., 2015). These measurements will be valuable in aiding our understanding of the geochemical reactivity expected for GCS and hydraulic fracturing activities in shale formations (Jun et al., 2013). In this study, we probe the surface interface interactions of CO_2 with the Utica Shale without water or fluid present using *in-situ* FT-IR spectroscopy, feature relocation SEM, BET surface area and pore size analysis, and quantitative adsorption isotherms. All reaction scenarios were examined at 40 °C and CO_2 pressures between 0 and 10.3 MPa.

3.2.1 In-situ FT-IR spectroscopy

In-situ FT-IR spectroscopy can discern vibrational changes in position and shape of the sorption bands sensitive to the gas-fluid-solid environment. For the Utica Shale sample, interaction of CO_2 was monitored as a function of increasing pressure with ATR-FT-IR spectroscopy (Figure

1). Upon exposure to the lowest CO_2 pressure (0.5 MPa), two broad absorption bands centered at 2343 and 2331 cm^{-1}, a shoulder at 2320 cm^{-1}, and a weak absorption region between 670 and 655 cm^{-1} were observed. These bands were monitored for 5 days; however, no changes were observed after the first 15 minutes of initial CO_2 exposure. As CO_2 pressure was increased in steps to 8.2 MPa, these bands grew in intensity. Scans at pressures above 3.0 MPa were left off Figures 1-3 to provide less crowded and easier to interpret plots. Higher pressure scans followed similar patterns.

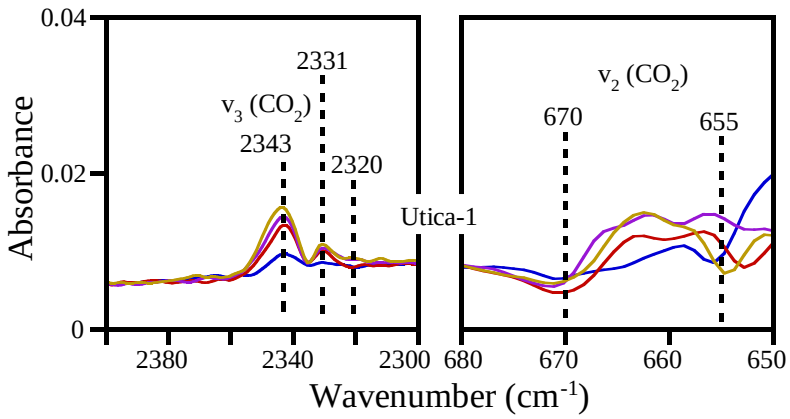

Figure 1. Utica Shale: Infrared spectra of the v_3 CO_2 asymmetric stretch (2343 and 2331 cm^{-1}) and v_2 CO_2 bending mode (670 to 655 cm^{-1}) of sorbed CO_2 as a function of increasing CO_2 pressure – 0.5 (blue), 1.5 (red), 2.2 (purple), and 3.0 (yellow) MPa.

For the clay standards of illite-smectite (mixed layer), illite, chlorite, and kaolinite, a very broad absorption band centered at 2343 cm^{-1}, a shoulder at 2320 cm^{-1}, and a weak absorption region between 670 and 655 cm^{-1} were observed (Figure 2). Again, as CO_2 pressure was increased in steps to 8.2 MPa, these bands grew in intensity for illite-smectite, illite, and chlorite. Absorption intensities were strongest for the illite-smectite standard, followed by illite, chlorite and kaolinite. Little to no absorption was apparent on the kaolinite clay standard. These observations are similar to previous work which examined surface condensation of CO_2 onto kaolinite and found that interactions are limited to the kaolinite surface and that initially CO_2 molecules lie parallel to the kaolinite surface followed by a distorted T-shape arrangement (Schaef et al., 2014). Additionally, this previous work found that the sorption process for CO_2 and clays appears to be unique for individual clay types (Schaef et al., 2014).

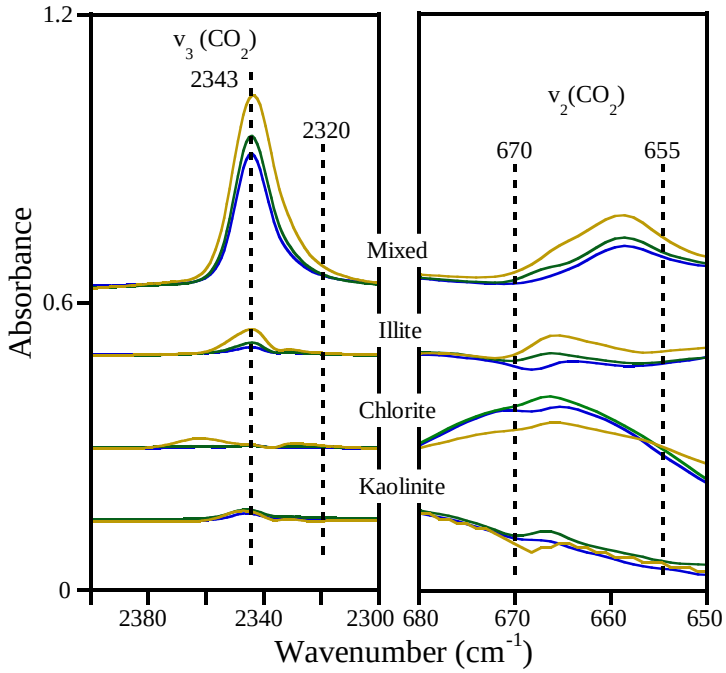

Figure 2. Illite-smectite (mixed layer), illite, chlorite, and kaolinite clays: Infrared spectra of the v_3 CO_2 asymmetric stretch (2343 cm^{-1}) and v_2 CO_2 bending mode (670 to 655 cm^{-1}) of sorbed CO_2 as a function of increasing CO_2 pressure – 0.5 (blue), 0.8 (green), and 3.0 (yellow) MPa.

For the dry kerogen sample, two adsorption bands centered at 2343 and 2331 cm^{-1}, a shoulder at 2320 cm^{-1} and a weak absorption region between 665 to 645 cm^{-1} were observed (Figure 3). As with the shale and clay samples, no changes were observed for the kerogen sample at the lowest CO_2 exposure after 15 minutes of data collection and the bands increased with pressure as CO_2 was increased from 0-8.2 MPa.

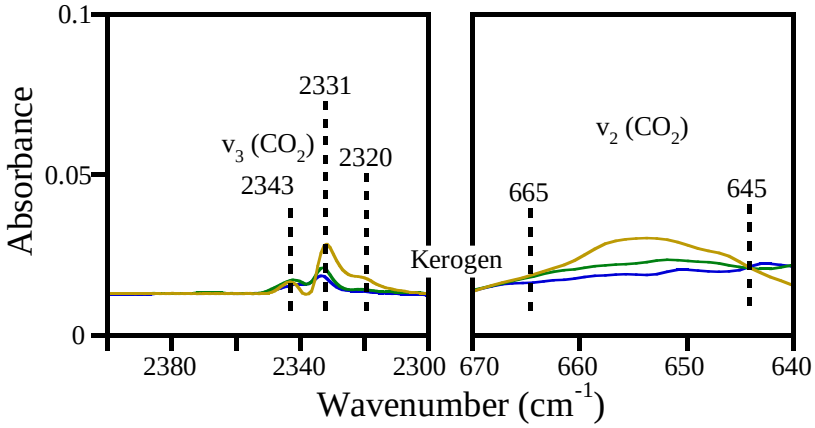

Figure 3. Kerogen: Infrared spectra of the v_3 CO_2 asymmetric stretch (2331 cm^{-1}) and v_2 CO_2 bending mode (665 to 645 cm^{-1}) of physical adsorbed/absorbed CO_2 as a function of increasing CO_2 pressure – 0.5 (blue), 0.8 (green), and 3.0 (yellow) MPa.

Free gas-phase CO_2 has two active infrared modes - a ν_3 anti-symmetric stretching mode at 2349 cm^{-1} and a ν_2 bending mode around 667 cm^{-1}. Upon interaction with a surface or interface, these free gas phase vibrations will exhibit a frequency shift that is representative of the chemical environment of the CO_2. It is important to note, that a single ν_3 anti-symmetric stretching mode represents a single environment for CO_2 interaction with a surface or interface. If other environments for CO_2 interaction are present, then additional ν_3 anti-symmetric stretching modes would be observable. The ν_2 CO_2 bending mode at ~667 cm^{-1} is a degenerate mode and can split into an in-plane bend at a lower frequency and an out-of-plane bend at a higher frequency upon an interaction with a surface or interface if the linear symmetry is distorted. The degree of degeneracy and distortion is directly related to the extent of the split of the in-plane and out-of-plane bend which can disclose details about the CO_2 environment such as Lewis base, Lewis acid, and electrostatic interactions. Lewis Base interactions tend to result in ν_3 blue-shifted bands between 2379-2340 cm^{-1} and ν_2 bands with little or no splitting (Xamena and Zecchina, 2002; Gregoire et al., 2003; Ricks et al., 2013; Dietzel et al., 2008) while Lewis acid interactions tend to produce ν_3 red-shifted bands between 2339-2335 cm^{-1} and ν_2 bands with moderate splitting (Kazarian et al., 1996; Nelson and Borkman,1998). Electrostatic interactions commonly result in a ν_3 red-shifted band between 2335-2332 cm^{-1} and ν_2 bands that are broad and undefined (Kazarian et al., 1996; Nelson and Borkman, 1998; Culp et al., 2010). The shoulder band at 2320 cm^{-1} has been observed when CO_2 is physically adsorbed with a surface and is assigned to the $\nu_3 + \nu_2 - \nu_2$ combination band (Culp et al., 2010).

The band positions observed with the Utica sample, clay standards, and kerogen sample (Figures 1-3) result in a slightly red-shifted ν_3 mode, the observance of a shoulder band, and a broad undefined ν_2 which are consistent with the observation of physically adsorbed/absorbed CO_2. The CO_2 molecule is weakly constrained with a surface or interface and is no longer able to freely rotate and is most consistent with weak electrostatic interactions between CO_2 and the interface. These vibrational assignments are consistent with observations of CO_2 interactions made

on similar materials such as coal (Goodman et al., 2005) and clays (Krukowski et al., 2015; Loring et al., 2014, 2012; Schaef et al., 2015).

The fact that two vibrational ν_3 modes at 2343 and 2331 cm^{-1} are detected for the Utica Shale suggests that two chemically different mechanisms exist for CO_2 interaction. The spectra for CO_2 interaction with the clay standards indicate that these CO_2-clay/inorganic interactions result in a frequency at 2343 cm^{-1} and are consistent with CO_2 interaction with other clay materials (Krukowski et al., 2015) and quartz structures (Kauffman et al., 2011). Two vibrational ν_3 modes at 2343 cm^{-1} and 2331 cm^{-1} are present in the spectra for CO_2 interaction with the kerogen. However, the kerogen sample is not pure and contains clay/quartz material as mentioned previously. Based on the CO_2/clay spectra, we can assign the band at 2343 cm^{-1} to CO_2 interacting with the impurities in the kerogen sample. The band at 2331 cm^{-1} is assigned to CO_2 interaction with the kerogen and is consistent with CO_2 interaction with organic materials such as coal (Goodman et al., 2005). However, it is important to note that these bands positions have also been observed for CO_2 in single-walled nanotubes/micropores and other host materials (Kauffman et al., 2011). For the Utica Shale, based on these observations we assign the vibrational bands at 2343 cm^{-1} and 2331 cm^{-1} to be representative of CO_2 interacting with clay mineral components and the kerogen matter in the Utica sample, respectively.

It is important to note that for the Utica Shale sample, additional changes (Figure 4) were observed at 1424 cm^{-1}, 874 cm^{-1}, and 712 cm^{-1} as a function of CO_2 pressure up to 6.9 MPa. These band positions are indicative of carbonate-like species with a ν_3 anti-symmetric band between 1500 and 1400 cm^{-1}, and ν_2 out-of-plane bend near 800 cm^{-1} and an ν_4 in-plane bend near 700 cm^{-1} (Pokrovsky et al., 2000) and most likely represent the presence of calcite ($CaCO_3$) as observed via SEM.

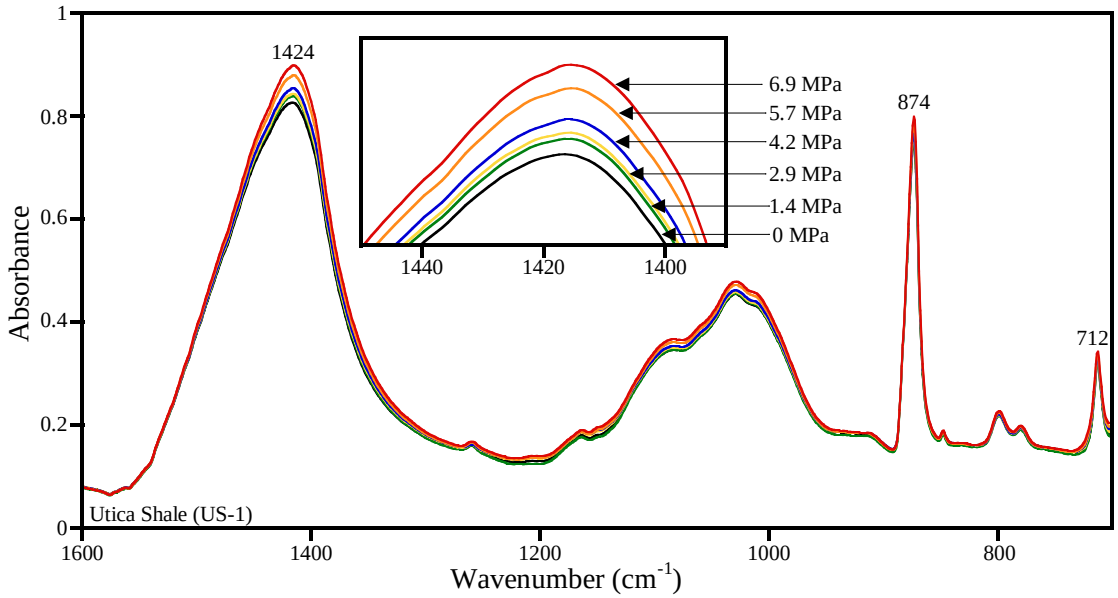

Figure 4. Carbonate formation as a function of increasing CO_2 pressure – 1.4, 2.9, 4.2, 5.7, and 6.9 MPa.

These carbonate bands were present initially before CO_2 exposure, however, the intensity of the bands changed slightly during CO_2 exposure. While the overall trend was an increase in intensity of the carbonate bands as a function of increasing pressure (Figure 4), the bands initially increased in intensity and then decreased for each CO_2 pressure level. It appears that in the process of adding increasing CO_2 pressure, carbonate precipitation and dissolution occurred until equilibrium was established. Lahann et al. (2013) documented that one of the first changes they observed upon interaction of CO_2 with New Albany shale was carbonate dissolution due to pH buffering. The infrared observations reported here likely document dynamic calcite dissolution and precipitation that has previously been observed (Lahann et al., 2013; Lu et al., 2016).

3.2.2 Feature relocation scanning electron microscopy

Surface relocation techniques via high-resolution field-emission scanning electron microscopy (FE-SEM) can be used to analyze and compare chemical and physical changes before and after exposure to CO_2 and fluids (Kutchko et al., 2013). The Utica Shale sample consisted predominantly of a calcite matrix with quartz grains and pyrite in the form of small, separate crystals. Very little organic content or clay was observed on the surface. No visible laminations or preferred orientation of minerals were observed and visible porosity was minor (Figure 5, left). In the unreacted SEM-BSE image, the black regions are pores, the darker grains labeled “Q” are the

quartz grains, the very bright grains labeled “Py” are pyrite, and the medium greyscale matrix is the calcite (not labeled). Mineral grain identification was performed using Energy Dispersive X-Ray Spectroscopy (EDS) which was only collected for specific points of interest. Not all quartz and pyrite grains are labeled in the images.

Once the Utica Shale was exposed to dry supercritical CO_2 for 14 days at storage conditions (40 °C and 10.3 MPa), etching and pitting with minor calcite precipitation were observed along the surface of the sample. Images in Figures 5-8 compare the exact same location before and after CO_2 exposure (left and right image, respectively). Figure 5 shows the calcite matrix, quartz and pyrite grains. Increased magnification shows significant etching and dissolution pits when compared with the images of the same samples before they were exposed which appears to be localized to the calcite matrix (Figures 6-8). Figure 6 highlights the dissolution pits in the calcite matrix while showing that the quartz grains appear unaffected/unreacted. Figure 7 displays the calcite matrix and etching. In some areas, the precipitation of calcium carbonate crystals can be seen along with the etching (Figure 8). Before and after images of quartz and pyrite features look unaltered and therefore do not appear to be impacted by exposure to supercritical CO_2.

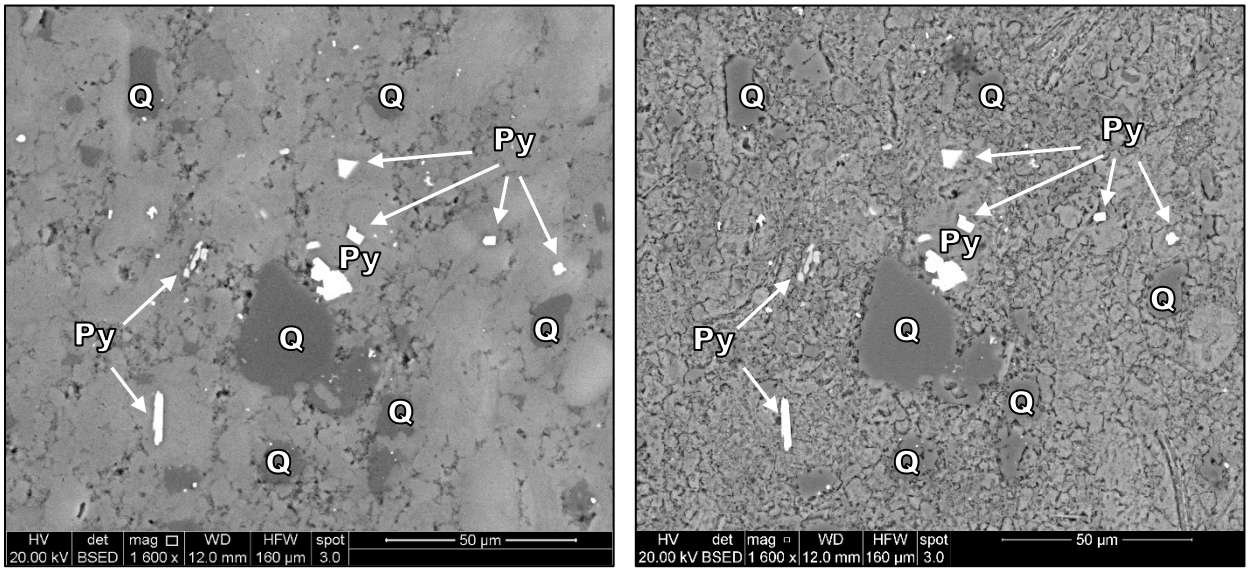

Figure 5. Scanning electron microscopy backscattered electron (BSE) images of unexposed Utica Shale (left) and dry supercritical CO_2 exposed Utica Shale (right). These images are of the same location before and after exposure. They primarily show the calcite matrix, quartz and pyrite grains. Etching is apparent in the exposed sample (right).

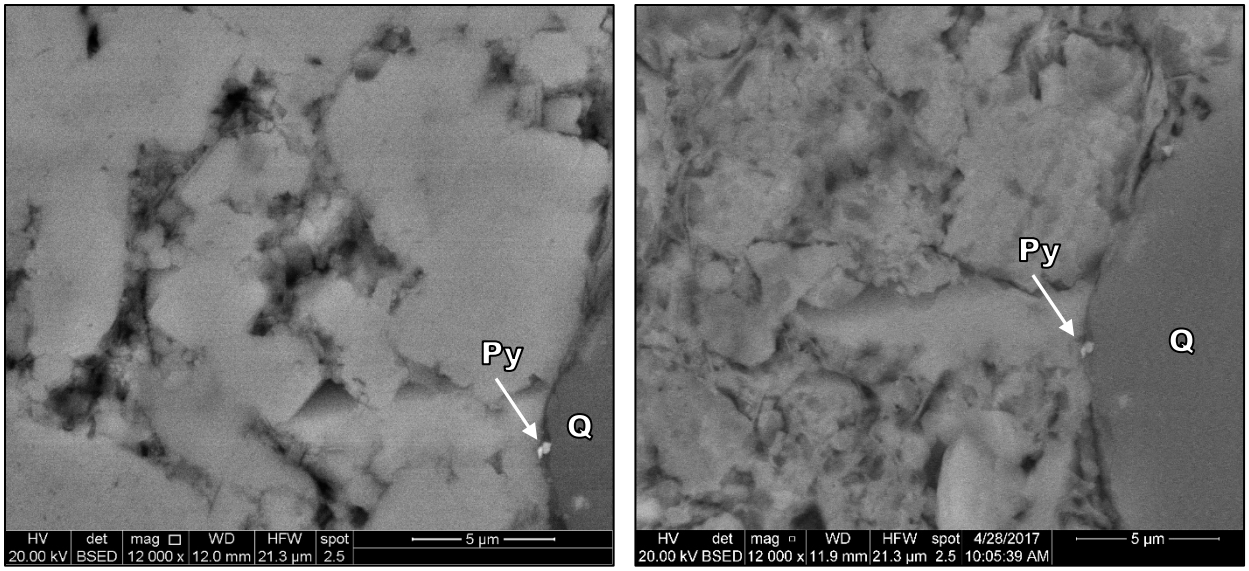

Figure 6. Scanning electron microscopy backscattered electron (BSE) images of unexposed Utica Shale (left) and dry supercritical CO_2 exposed Utica Shale (right). These images are of the same location before and after exposure and contain primarily the calcite matrix. Notice the dissolution pits in the calcite matrix. The quartz displays no visible signs of alteration.

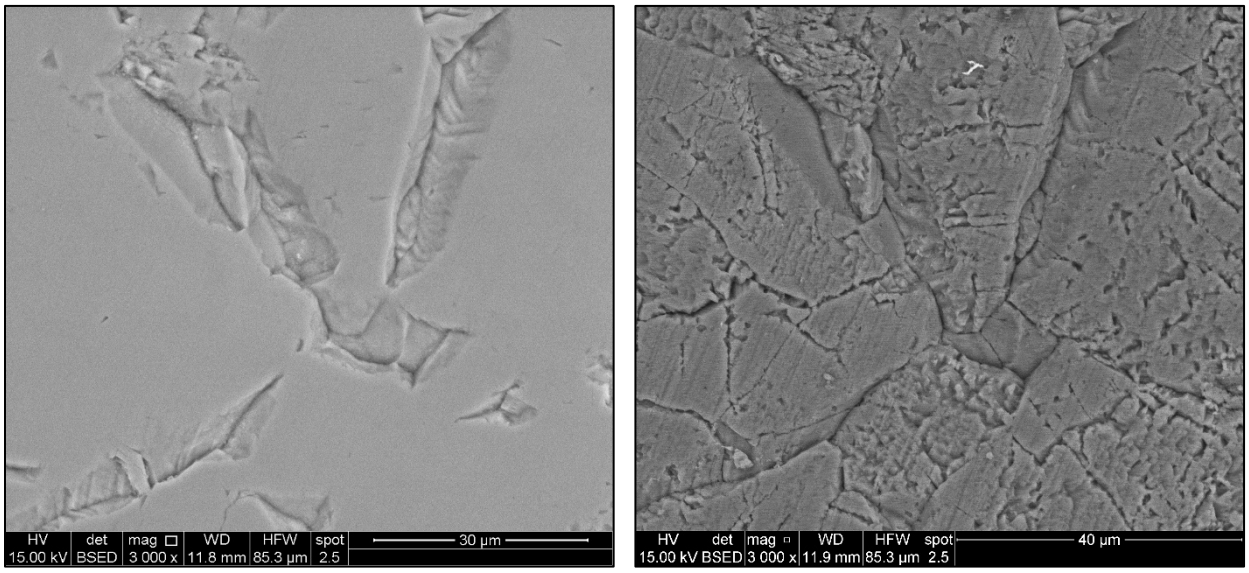

Figure 7. Scanning electron microscopy backscattered electron (BSE) images of unexposed Utica Shale (left) and dry supercritical CO_2 exposed Utica Shale (right) showing the calcite matrix. These images are of the same location before and after exposure. These images provide further evidence of calcite dissolution and etching. Note the extensive pitting in the calcite matrix in the right image.

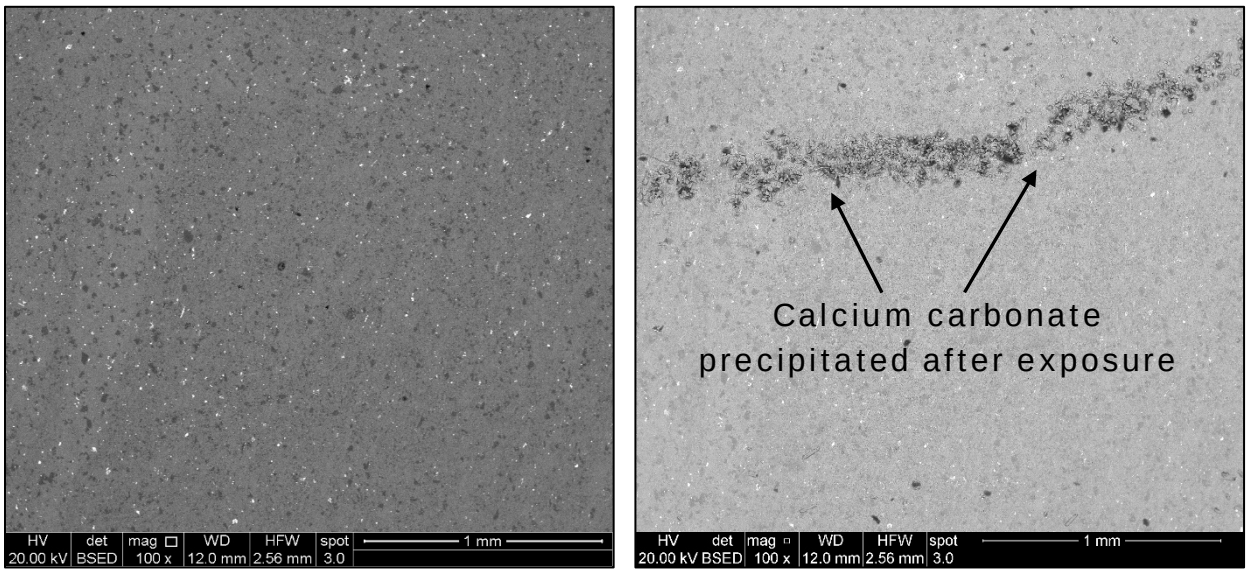

Figure 8. Low magnification scanning electron microscopy backscattered electron (BSE) images of unexposed Utica Shale (left) and dry supercritical CO_2 exposed Utica Shale (right). These images are of the same location before and after exposure and show calcium carbonate crystals precipitated by the exposure of dry supercritical CO_2.

3.2.3. Brunauer-Emmett-Teller surface area and pore size analysis

Combined N_2 and CO_2 isotherm characterization was carried out to determine BET surface area and micro- and mesopore volume/size distribution of unexposed and CO_2-exposed US-1 sample. As shown in Figure 9A and 9B, N_2 isotherms at -196 °C demonstrate combined Type I(b) and Type IV(a), indicative of micro- and mesoporosity of the materials (Thommes et al., 2015). No plateau was observed at the upper P/P_0 range of the adsorption isotherm (Figure 9A and 9B), indicating that the pore network consists of larger pores that cannot be completely filled via N_2 adsorption. Without an observable plateau, we were unable to determine the total pore volume and macropore volume. It is worth nothing that the macro-porosity observed with the SEM analysis (Figures 5-7) appeared to increase after CO_2 exposure with dissolution and etching. Swelling of the clay component of the shale occurs during gas adsorption as suggested by the fact that the N_2 adsorption and desorption isotherms do not overlay completely at the lower P/P_0 range. This phenomenon has also been reported with other shale samples (Firouzi et al., 2014; Kuila et al., 2014; Yang et al., 2016; Jiang et al., 2016). It is likely the illite-smectite (mixed layer) and/or kerogen are contributing to swelling observed in this work. Furthermore, the associated hysteresis loop provides information about the pore connectivity. The N_2 isotherms exhibit Type H3/H4 loop

with cavitation, which is typical of shale. The cavitation step points out that the mesopores are only accessible through the narrow micropores (Thommes and Cychosz, 2014).

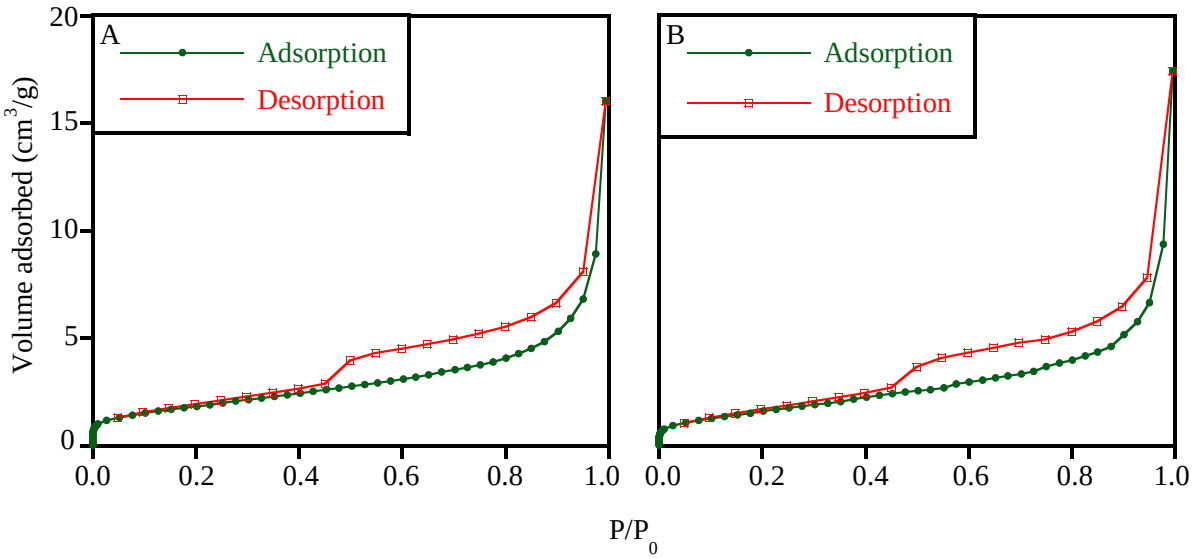

Figure 9. N_2 adsorption-desorption isotherms at -196 °C for (A) unexposed and (B) CO_2-exposed US-1.

Application of DFT methods allows an accurate pore size analysis of micro- and mesoporous materials. Table 5 summarizes the textural properties of the Utica Shale before and after CO_2 exposure based on N_2 -196 °C and CO_2 0 °C measurements. Although the BET surface area of the Utica Shale sample (6.8 m^2/g) remains relatively the same after CO_2 exposure (6.3 m^2/g), the micropore surface area and volume from the N_2 -196 °C measurements noticeably decreases from 1.4 to 0.4 m^2/g (71% decrease) and 0.00071 to 0.00030 cm^3/g (58% decrease), respectively. Smaller changes were observed in the meso-pore and ultramicro-pore volumes (Table 5). The CO_2 adsorption isotherm, pore size distribution, and cumulative pore volume obtained by applying the QSDFT and NLDFT are illustrated in Figures 10A, 10B, and 10C. The experimental N_2 isotherm and theoretical QSDFT isotherm are compared in Figure 10D. Overall, the DFT calculations are in agreement with the experimental data, as the fitting error ranges between 0.2 and 1%. The plots for the CO_2-exposed sample are not shown as they look very similar to those for the unexposed sample.

Table 5. Textural properties of unexposed and CO_2-exposed US-1 samples.

Parameter	*Unexposed*	*CO_2-exposed*
BET surface area (m^2/g)	6.8	6.3
Micropore surface area (m^2/g)[a]	1.4	0.4
Micropore volume (cm^3/g)[a]	0.00071	0.00030
Ultramicropore volume (cm^3/g)[b]	0.00127	0.00141
Total micropore volume (cm^3/g)	0.00198	0.00171
Mesopore volume (cm^3/g)[c]	0.01177	0.01239
Fitting error for N_2 -196 °C (%)	0.57	0.98
Fitting error for CO_2 0 °C (%)	0.18	0.26

[a]N_2 -196 °C, QSDFT, pore width = 0.7-2 nm.
[b]CO_2 0 °C, NLDFT, pore width < 0.7 nm.
[c]N_2 -196 °C, QSDFT, pore width = 2-50 nm.

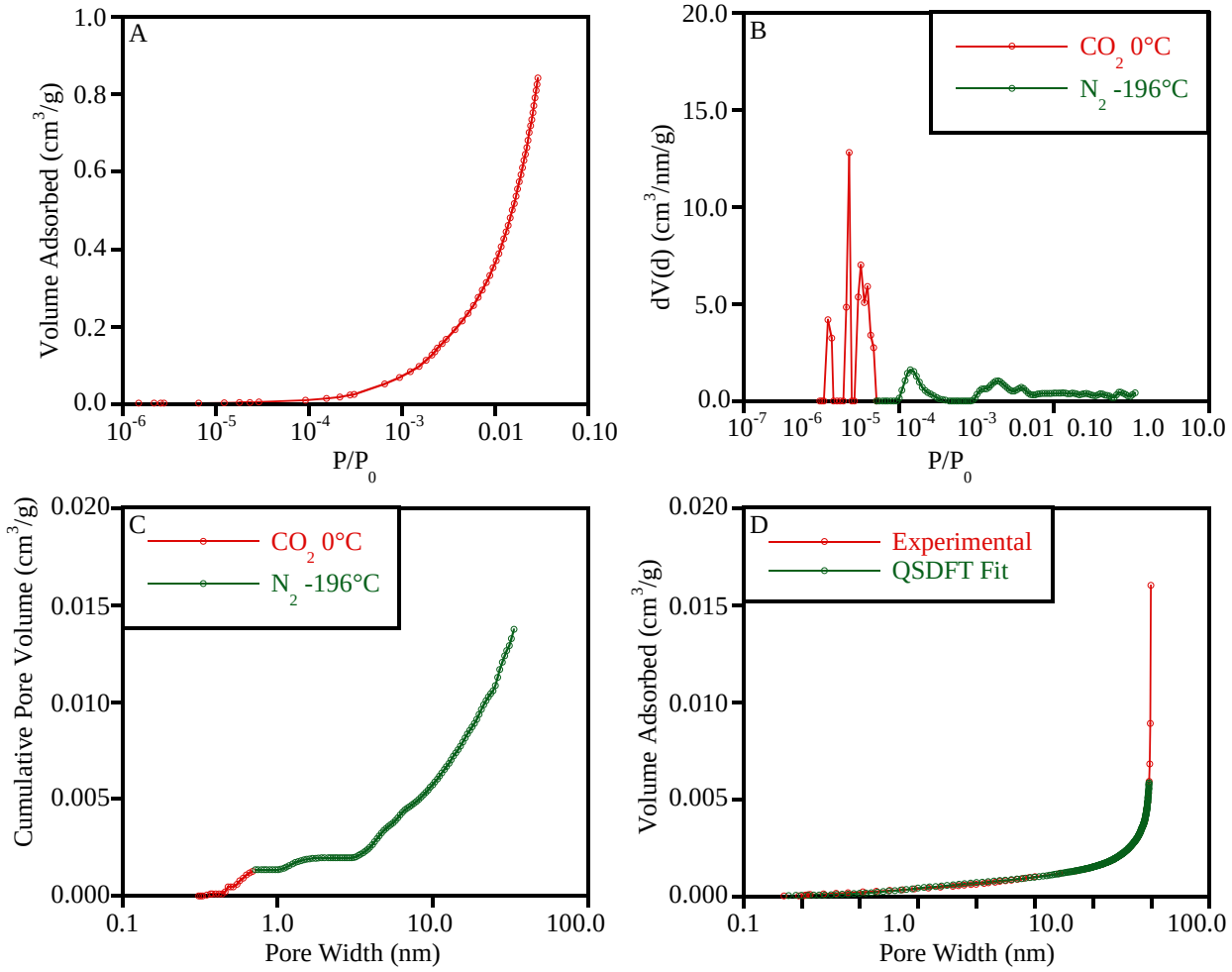

Figure 10. Unexposed US-1 sample: (A) CO_2 adsorption isotherm at 0 °C, (B) pore size distribution, (C) cumulative pore volume, and (D) comparison between experimental N_2 isotherm and QSDFT fit.

3.2.4 Quantitative adsorption isotherms

To further explore the CO_2 adsorption behavior of the Utica Shale, the CO_2 adsorption isotherm was measured at -25 °C up to a pressure of 1.5 MPa. This temperature was chosen to provide the maximum range of relative pressure (0-0.9 P/P_0) within the 1.6 MPa pressure limit of the instrument. The wide range of P/P_0 at low temperature provides a good estimate of the expected CO_2 adsorption behavior at the higher pressure and temperature environments which would be encountered during geologic storage. The adsorption isotherm for the unexposed US-1 sample, is shown in Figure 11. The volumetric adsorption of CO_2 in the sample is similar to the volumetric adsorption of N_2 observed at -196 °C over a similar relative pressure range as shown

in Figure 9. No fine structure in the CO_2 isotherm is observable since the CO_2 uptake in the US-1 sample is near the 1 cm^3/g resolution of the instrument; however, there appears to be a similar sharp initial uptake of ~ 1 cm^3/g CO_2 in the lower P/P_0 range of the isotherm followed by a shallow positive slope over the remainder of the isotherm. This behavior is indicative of a combination of micropores filling in the low P/P_0 region followed by mesopores filling at higher relative pressures as concluded from the N_2 BET analysis.

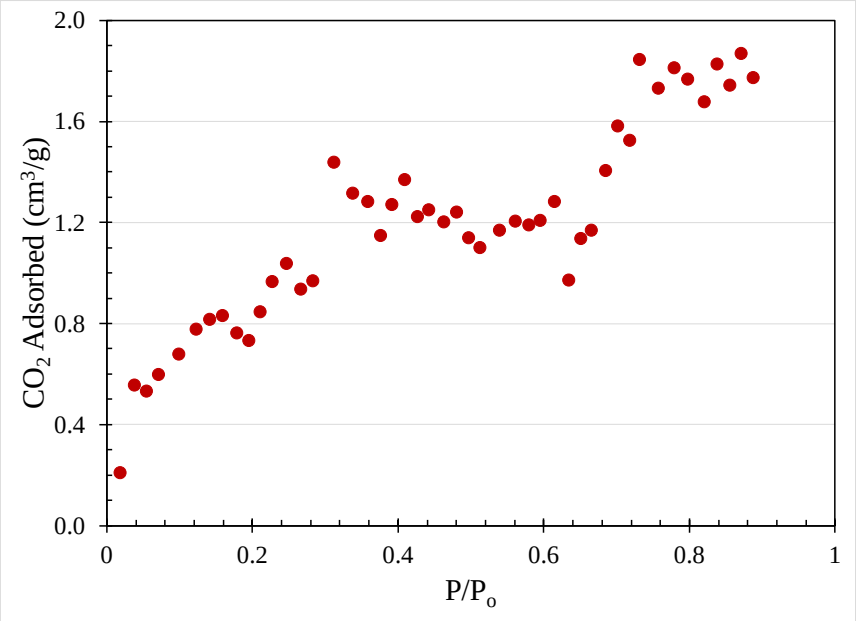

Figure 11. Volumetric adsorption isotherm for CO_2 on shale sample, US-1, measured at -25 °C.

Adsorption isotherms for CO_2 were also measured over similar P/P_0 ranges for illite-smectite (mixed layer), illite, chlorite, kaolinite, and kerogen neat samples of the primary constituents of the Utica Shale as listed in Table 2. The CO_2 adsorption isotherms for the constituents are compared to the shale adsorption isotherm in Figure 12. All the shale components show higher uptakes of CO_2 individually than what was observed in the bulk Utica Shale. This result indicates that many of the constituents in the shale are inaccessible to CO_2 even when the shale is ground to a fine powder. The amount of CO_2 adsorbed by the kerogen extract is significantly higher than any of the clays, particularly in the low relative pressure region. It can be concluded from the high uptake of CO_2 in the low P/P_0 region that the kerogen contains a higher fraction of micropores compared to the clays. The organic character of the kerogen likely also provides a favorable interaction for CO_2. It is also possible that the surface

area of the kerogen material was altered as a result of the extraction process causing the enhanced adsorption. The next highest sorbent in terms of CO_2 capacity is the mixed layer illite-smectite which shows a CO_2 capacity well above the other clays and is consistent with results observed by *in-situ* FT-IR spectroscopy analyses in this study and others (Krukowski et al., 2015; Loring et al., 2014, 2012; Schaef et al., 2015). In addition, the CO_2 adsorption isotherm for the illite-smectite material undergoes a noticeable upturn in the high P/P_0 region indicative of a Type IIb isotherm often observed during the adsorption of nonpolar gases in smectites. The illite, chlorite, and kaolinite clay samples all showed similar low uptakes of CO_2 as was also observed by the *in-situ* FT-IR spectroscopy analysis in this study. Based on a qualitative analysis of the isotherm measurements, it can be concluded that shales with a higher content of kerogen and illite-smectite clays would be expected to have the highest CO_2 storage capacity, provided these constituents were accessible to the gas.

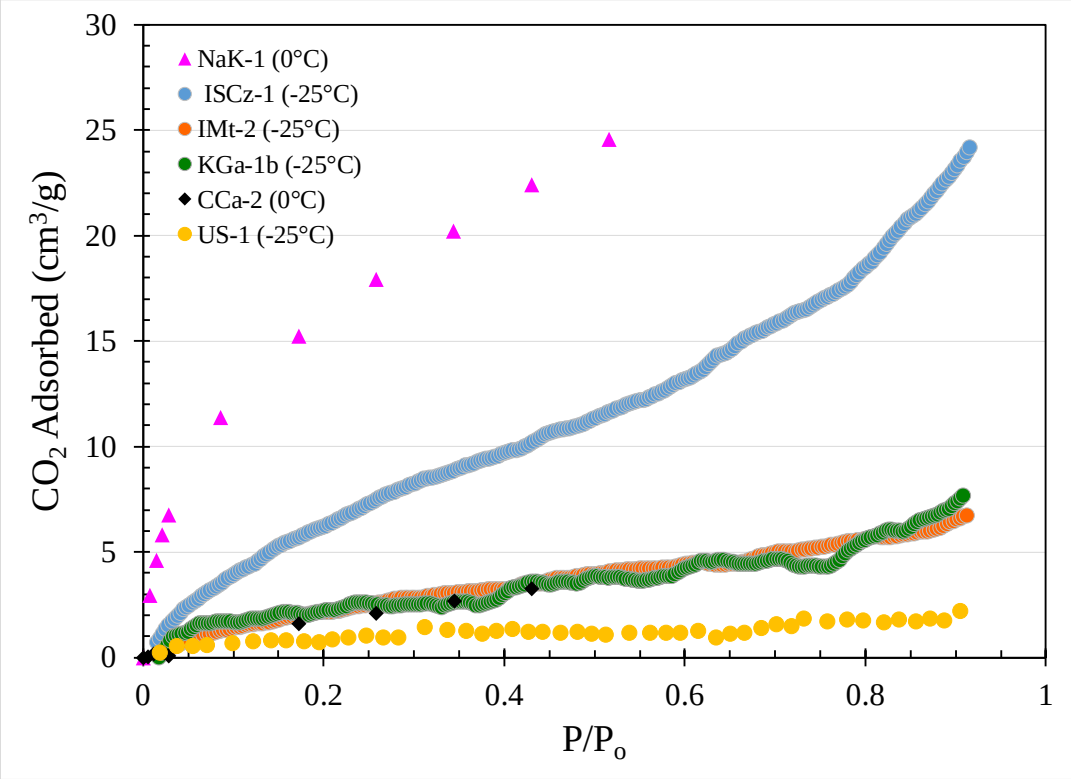

Figure 12. Comparing CO_2 adsorption isotherms for the US-1 shale sample to the various clay [mixed layer illite-smectite (ISCz-1), illite (IMt-2), chlorite (CCa-2) and kaolinite (KGa-1b)] and kerogen (NAk-1) components typically found in shale (see Table 2). Note that data for NAk-1 and CCa-2 were collected gravimetrically using a microbalance at -200 °C. The remaining samples are measured at -25 °C using a volumetric Sievert apparatus.

4. Environmental implications

The vast majority of experiments in the literature focus on CO_2-brine-rock interactions and it is often assumed that dry supercritical CO_2 does not interact with or have any impact on reservoir rocks or seals (Lahann et al., 2013; Shaef et al., 2014; Lu et al., 2016) and there are almost no studies on CO_2-induced changes in mineralization or dissolution for dry shale or pure minerals (McGrail et al., 2009). The literature indicates that CO_2 sorption in shales is correlated with organic content and sometimes clay content (Busch et al., 2008). The *in-situ* infrared spectroscopy results reported here show specific vibrational interactions of CO_2 with clay/quartz (2343 cm^{-1}) and kerogen (2331 cm^{-1}), components found in the Utica Shale. The quantitative adsorption isotherms indicate that shale with a higher content of kerogen and illite-smectite clays would be expected to have the highest CO_2 storage potential provided these constituents were accessible to CO_2.

The prevailing thought is that an aqueous phase is needed for any chemical alteration or reaction to proceed. It has been documented that a threshold concentration of water is needed at the interface for carbonation and dissolution reactions to occur (Loring et al., 2014; Schaef et al., 2013). Thompson et al. (2013) explains that water films play a critical role in that water reacts with CO_2 to produce carbonic acid to form protons and bicarbonate ions, promotes dissolution of silicate minerals, and provides a transport media and solvent for ion species. This becomes especially important in low water scenarios (Loring et al., 2014). In pore spaces of subsurface samples, water films and water concentrations will control the mineral carbonation extent and reactivity (Miller et al., 2013).

Only one other study was found to look at the interaction of dry supercritical CO_2 – with a reservoir formation (Lu et al., 2016). In this previous work, researchers also observed dissolution pits, corrosion, and etching in the calcite of their Middle Bakken samples. In addition, they observed some localized precipitation of calcite. This calcite precipitation was described as being likely facilitated by the presence of water retained in the interstitial pore space that had evaporated (wicked) into the supercritical CO_2. Despite the insignificant quantity of water available, the authors observed carbonate mineral surfaces were significantly etched. It was suggested that the water vapor may have formed a thin film only a few nanometers thick that facilitated the mineral reactions (Lu et al., 2016). Lahann et al. (2013) also observed etching by CO_2 on the New Albany shale, however, in the presence of a NaCl brine and pressure up to 24 MPa and noted that carbonate dissolution is one of the first responses upon CO_2 injection. The etching of carbonate seen in this

study with feature relocation SEM under dry conditions is very similar to that seen in Lu et al. (2016) and is likely facilitated by water retained in the interstitial pore space and matrix that had been extracted into the supercritical CO_2. In addition, the buffering effect of dissolution and re-precipitation of carbonates observed with *in-situ* infrared spectroscopy further supports the feature relocation SEM analysis.

It is not yet known how this etching impacts the overall permeability (and other physical behaviors) of the rock over time. However, it is reported in the literature that CO_2-induced dissolution and mineralization of carbonate minerals in fractures and faults may (1) increase or decrease permeability, (2) alter sorption, porosity, and molecular diffusion coefficients, and (3) potentially release material such as clays that may clog fracture networks or weaken fracture surfaces (Bourg et al., 2015). The alteration of these properties could affect future CO_2 storage activities and/or the use of CO_2 as a hydraulic fracturing media. In this work, both the BET surface area/pore size analysis and quantitative adsorption isotherm results stress that sorption is taking place in the micro- and meso-porosity of the Utica Shale and that the mesopores may only be accessible through the narrow micropores. In addition, the micropore surface area and volume decreased significantly after CO_2 exposure, possibly altering overall permeability and fracture networks. Further alteration was identified with the BET surface area and pore size analysis, as the swelling that occurs during CO_2 adsorption leads to hysteresis in sorption cycles. Further studies investigating the Utica and other shale formations are warranted to scale up from laboratory observations to field operations.

5. Conclusions

As research efforts focus on CO_2-brine-rock interactions with the assumption that dry supercritical CO_2 does not interact with or have any impact on reservoir rocks or seals, these results presented here indicate that dry supercritical CO_2 can alter the properties of shale formations. In this work with the Utica Shale, we showed that CO_2 does interact physically and reversibly with both kerogen and clay components of the shale with *in-situ* infrared spectroscopy and quantitative adsorption isotherms. In addition, our feature relocation scanning electron microscopy and *in-situ* infrared spectroscopy showed that CO_2 etches the Utica Shale surfaces by cycling between carbonate dissolution and precipitation which is likely facilitated by water retained in the interstitial pore space and matrix. The BET surface area/pore size analysis and

quantitative adsorption isotherms results both indicate that the micro- and meso-porosity of the Utica Shale is important for sorption and that the mesopores may only be accessible through the narrow micropores. Decreases in the micropore surface area and volume after CO_2 exposure may alter permeability and fracture network pathways. In addition, the BET surface area and pore size analysis identified that swelling occurs during N_2 adsorption leading to hysteresis in sorption cycles. Further studies are warranted to investigate CO_2-shale interactions and changes in rock properties that will impact both storage of anthropogenic CO_2 and hydraulic fracturing.

Acknowledgements

We would like to graciously thank Maria Mastalerz at Indiana University and Indiana Geologic Survey in Bloomington, IN for providing a kerogen sample extracted from the New Albany Shale. This technical effort was performed in support of the National Energy Technology Laboratory's ongoing research under the RES contract DE-FE0004000.

Disclaimer

This project was funded by the Department of Energy, National Energy Technology Laboratory, an agency of the United States Government, through a support contract with AECOM. Neither the United States Government nor any agency thereof, nor any of their employees, nor AECOM, nor any of their employees, makes any warranty, expressed or implied, or assumes any legal liability or responsibility for the accuracy, completeness, or usefulness of any information, apparatus, product, or process disclosed, or represents that its use would not infringe privately owned rights. Reference herein to any specific commercial product, process, or service by trade name, trademark, manufacturer, or otherwise, does not necessarily constitute or imply its endorsement, recommendation, or favoring by the United States Government or any agency thereof. The views and opinions of authors expressed herein do not necessarily state or reflect those of the United States Government or any agency thereof.

References

Bacon, D.H. Yonkofski, C.M.R., Schaef, H.T., White, M.D., McGrail, B.P., 2015. CO_2 storage by sorption on organic matter and clay in gas shale. Journal of Unconventional Oil and Gas Resources, v. 12, p. 123–133.

Bourg, I.C., Beckingham, L.E., DePaolo, D.J., 2015. The nanoscale basis of CO_2 trapping for geologic storage. Environ. Sci. Technol., v. 49, p. 10265-10284.

Busch, A., Alles, S., Gensterblum, Y., Prinz, D., Dewhurst, D.N., Raven, M.D., Stanjek, H., Krooss, B.M., 2008. Carbon dioxide storage potential of shales. Int. J. of Greenhouse Gas Control v. 2, p. 297-308.

Culp, J.T., Goodman, A.L., Chirdon, D., Sankar, S.G., Matranga, C., 2010. Mechanism for the Dynamic Adsorption of CO_2 and CH_4 in a Flexible Linear Chain Coordination Polymer as Determined from In Situ Infrared Spectroscopy, J. Phys. Chem., v. 114 (5), p. 2184-2191.

Dieterich, M., Kutchko, B., Goodman, A., 2016. Characterization of Marcellus Shale and Huntersville Chert before and after exposure to hydraulic fracturing fluid via feature relocation using field-emission scanning electron microscopy. Fuel, v. 182, p. 227-235.

Dietzel, P.D.C., Johnsen, R.E., Fjellvag, H., Bordiga, S., Groppo,E., Chavan, S., Blom, R., 2008. Adsorption properties and structure of CO_2 adsorbed on open coordination sites of metal organic framework Ni(2)(dhtp) from gas adsorption, IR spectroscopy, and X-ray diffraction. Chem. Commun., p. 5125-5127.

Emmons, E., 1842. Geology of New York; Part II, Survey of the second geological district. New York State Museum, p. 437.

Firouzi, M., Rupp, E.C., Liu, C.W., Wilcox, J., 2014. Molecular simulation and experimental characterization of the nanoporous structures of coal and gas shale. Int. J. Coal Geology, v. 121, p. 123-128, https://doi.org/10.1016/j.coal.2013.11.003.

Goodman, A. L., Campus, L. M., Schroeder, K. T., 2005. Direct Evidence of Carbon Dioxide Sorption on Argonne Premium Coals Using ATR-FTIR Spectroscopy. **Energy & Fuels**, v. *19*, p. 471-476.

Gregoire, G., Brinkmann, N.R., van Heijnsbergen, D., Schaefer, H.F., Duncan, M.A., 2003. Infrared photodissociation spectroscopy of Mg+(CO_2)n and Mg+ (CO_2)n Ar clusters. J. Phys. Chem. A v. 107, p. 218–227.

Hosterman, J.W., Whitlow, S.T., 1983. Clay Mineralogy of Devonian Shales in the Appalachian Basin. Geological Survey Open-File Rep. p. 81-585.

Hulver, M.L., 1997. Post-orogenic evolution of the Appalachian mountain system and its foreland: Chicago, Illinois, University of Chicago, Ph.D. dissertation, p. 1055.

Iwai, Y., Murozono, T., Koujina, Y., Arai, Y., Sakanishi, K., 2000. Physical properties of low rank coals dried with supercritical carbon dioxide. *J. Supercrit. Fluids*, v. 18, p. 73-79.

Jacobs, T., 2014. Energized fractures: shale revolution revisits the energized fracture. J. Pet. Technol. 66, v. 6, p. 48-56.

Jarvie, D.M., 2012. Shale resource systems for oil and gas: Part 1—shale-gas resource systems. AAPG Memoir, v. 97, p. 69-87.

Jiang, F., Chen, D., Chen, J., Li, Q., Liu, Y., Shao, X., Hu, T., Dai, J., 2016. Fractal analysis of shale pore structure of continental gas shale reservoir in the Ordos Basin, NW China. Energy & Fuels. v. 30, p. 4676-4689, http://pubs.acs.org/doi/abs/10.1021/acs.energyfuels.6b00574.

Jun, Y., Giammar, D.E., Werth, C.J., 2013. Impacts of geochemical reactions on geologic carbon sequestration. Environ. Sci. Technol. v. 47, p. 3-8.

Kauffman, K. L., Culp, J. T., Goodman, A. L., Matranga, C. 2011. FT-IR Study of CO_2 adsorption in a dynamic Copper(II) Benzoate-Pyrazine Host with CO_2-CO_2 interactions in the adsorbed state. J. Phys. Chem. C., v. 115, p. 1857–1866.

Kazarian, S.G., Vincent, M.F., Bright, F.V., Liotta, C.L. Eckert, C.A.J., 1996. Specific intermolecular interaction of carbon dioxide with polymers. Am. Chem. Soc. v. 118, p. 1729-1736.

Krukowski, E.G., Goodman, A., Rother, G., Ilton, E.S., Guthrie, G., Bodnar, R.J., 2015. FT-IR study of CO_2 interaction with Na+ exchanged montmorillonite. Appl. Clay Sci. v. 114, p. 61–68, http://dx.doi.org/10.1016/j.clay.2015.05.005.

Kuila, U., McCarty, D.K., Derkowski, A., Fischer, T.B., Topòr, T., Prasad, M., 2014. Fuel. v. 135, p. 359-373, https://doi.org/10.1016/j.fuel.2014.06.036.

Kutchko, B.G., Goodman, A.L., Rosenbaum, E., Natesakhawat, S., Wagner, K., 2013. Characterization of coal before and after supercritical CO_2 exposure via feature relocation using field-emission scanning electron microscopy. Fuel, v. 107, p. 777-786.

Lahann, R., Mastalerz, M., Rupp, J.A., Drobniak, A., 2013. Influence of CO_2 on New Albany Shale composition and pore structure. International Journal of Coal Geology, v. 108, p. 2-9.

Lee, M-S., McGrail, B.P., Rousseau, R., Glezakou, V-A., 2015. Structure, dynamics and stability of water/scCO_2/mineral interfaces from *ab initio* molecular dynamics simulations. Scientific Reports, v. 5, No. 14857.

Lemmon, E.W., Huber, M.L., McLinden, M.O., 2013. NIST standard reference database 23: NIST reference fluid thermodynamic and transport properties—REFPROP. Version 9.1. Standard Reference Data Program, Gaithersburg, Maryland.

Levine, J.S., Fukai, I. Soeder, D.J., Bromhal, G., Dilmore, R.M., Guthrie, G.D., Rodosta, T., Sanguinito, S., Frailey, S., Gorecki, D., Peck, W., Goodman, A.L., 2016. U.S. DOE NETL

methodology for estimating the prospective CO_2 storage resource of shales at the national and regional scale. International Journal of Greenhouse Gas Control, v. 51, p. 81-94.

Liu, F., Ellett, K., Xiao, Y., Rupp, J.A., 2013. Assessing the feasibility of CO_2 storage in the New Albany Shale (Devonian-Mississippian) with potential enhanced gas recovery using reservoir simulation. International Journal of Greenhouse Gas Control, v. 17, p. 111-126.

Loring, J.S., Schaef, H.T., Turcu, R.V.F., Thompson, C.J., Miller, Q.R.S., Martin, P.F., Hu, J., Hoyt, D.W., Qafoku, O., Ilton, E.S., Felmy, A.R., Rosso, K.M., 2012. *In situ* molecular spectroscopic evidence for CO_2 intercalation into montmorillonite in supercritical carbon dioxide. Langmuir 28, v. 18, p. 7125–7128, http://dx.doi.org/10.1021/la301136w.

Loring, J.S., Ilton, E.S., Thompson, C.J., Martin, P.F., Rosso, K.M., Felmy, A.R., Schaef, H.T., 2014. In situ study of CO_2 and H_2O partitioning between Na-montmorillonite and variably wet supercritical carbon dioxide. Langmuir 30, v. 21, p. 6120–6128.

Loucks, R.G., Reed, R.M., Ruppel, S.C., Jarvie, J.M., 2009. Morphology, genesis and distribution of nanometer-scale pores in siliceous mudstones of the Mississippian Barnett Shale. Journal of Sedimentary Research, v. 79, p. 848-861.

Lu, J., Nicot, J.P., Mickler, P.J., Ribeiro, L.H., Darvari, R., 2016. Alteration of Bakken reservoir rock during CO_2-based fracturing—An autoclave reaction experiment. Journal of Unconventional Oil and Gas Resources, v. 14, p. 72-85.

McGrail, B., Schaef, H., Glezakou, V., Dang, L., Owen, A., 2009, Water reactivity in the liquid and supercritical CO2 phase: Has half the story been neglected? Energy Procedia, v. 1, p. 3415-3419, https://dx.doi.org/10.1016/j.egypro.2009.02.131.

Miller, Q.R.S., Thompson, C.J., Loring, J.S., Windisch, C.F., Bowden, M.E., Hoyt, D.W., Hu, J.Z., Arey, B.W., Rosso, K.M., Schaef, H.T., 2013. Insights into silicate carbonation processes in water-bearing supercritical CO_2 fluids. Int. J. Greenhouse Gas Control, v. 15, p. 104–118, http://dx.doi.org/10.1016/j.ijggc.2013.02.005.

Nelson, M. R., Borkman, R.F.J., 1998. Ab initio calculations on CO2 binding to carbonyl groups. J. Phys. Chem. A., v. 102, p. 7860-7863.

Orr, F.M., 2009a. CO_2 capture and storage: are we ready? Energy Environ.Sci. v. 2 (5), p. 449-458.

Orr, F.M. 2009b. Onshore geologic storage of CO_2. Science, v. 325, p. 1656-1658.

Pokrovsky, O.S., Mielczarski, J.A., Barres, O., Schott, J., 2000. Surface speciation models of calcite and dolomite/aqueous solution interfaces and their spectroscopic evaluation. Langmuir 16, v. 6, p. 2677-2688.

Pollastro, R.M., 1993. Considerations and applications of the illite/smectite geothermometer in hydrocarbon-bearing rocks of Miocene to Mississippian age. Clays Clay Miner, v. 41, p. 119-133.

Pruess, K., Müller, N., 2009. Formation dry-out from CO_2 injection into saline aquifers: 1. Effects of solids precipitation and their mitigation. Water Resources Research, v. 45, W03042-1–W03042-11. http://dx.doi.org/10.1029/2008WR007101.

Ricks, A.M., Brathwaite, A.D., Duncan, M.A., 2013. IR spectroscopy of gas phase $V(CO_2)n^+$ clusters: solvation-induced electron transfer and activation of CO_2. J. Phys. Chem. A, v. 117, p. 11490-11498.

Romanov, V., Soong, Y., Carney, C., Rush, G.E., Nielsen, B., O'Connor, W., 2015. Mineralization of carbon dioxide: A literature review. Chem. Bio. Eng. Rev., v. 2, No. 4, p. 231-256.

Ross, D.J.K., Bustin, R.M., 2007. Shale gas potential of the Lower Jurassic Gordondale Member, northeastern British Columbia, Canada. Bulletin of Canadian Petroleum Geology, v. 55, p. 51-75.

Ross, D.J.K., Bustin, R.M., 2008, Characterizing the shale gas resource potential of Devonian-Mississippian strata in the Western Canada sedimentary basin: Application of an integrated formation evaluation. AAPG Bulletin, v. 92, p. 87-125.

Ross, D.J.K., Bustin, R.M., 2009. The importance of shale composition and pore structure upon gas storage potential of shale gas reservoirs. Marine and Petroleum Geology, v. 26, p. 916-927.

Rother, G., Ilton, E.S., Wallacher, D., Haub, T., Shaef, H.T., Qafoku, O., Rosso, K.M., Felmy, A.R., Krukowski, E.G., Stack, A.G., Grimm, N., Bodnar, R.J., 2013, Environmental Science and Technology, v. 47, p. 205-211.

Roychaudhuri, B., Tsotsis, T.T., Jessen, K., 2013. An experimental investigation of spontaneous imbibition in gas shales. Journal of Petroleum Science and Engineering, v. 111, p. 87-97.

Rowan, E.L., 2006. Burial and thermal history of the Central Appalachian Basin, based on three 2-D models of Ohio, Pennsylvania, and West Virginia. USGS Open-File Report, v. 1019, p. 37.

Schaef, H.T., Glezakou, V.A., Owen, A.T., Ramprasad, S., Martin, P.F., McGrail, B.P., 2014. Surface Condensation of CO_2 onto Kaolinite. Environ. Sci. Technol. Lett., v. 1, p. 142-145.

Schaef, H.T., Loring, J.S., Glezakou, V.A., Miller, Q.R.S., Chen, J., Owen, A.T., Lee, M.S., Ilton, E.S., Felmy, A.R., McGrail, B.P., Thompson, C.J., 2015. Competitive sorption of CO_2 and H_2O in 2:1 layer phyllosilicates. Geochim. Cosmochim. Acta, v. 161, p. 248-257, http://dx.doi.org/10.1016/j.gca.2015.03.027.

Schaef, H.T., Miller, Q.R.S., Thompson, C.J., Loring, J.S., Bowden, M.S., Arey, B.W., McGrail, B.P., Rosso, K.M., 2013. Silicate carbonation in supercritical CO_2 containing

dissolved H_2O: An *in situ* high pressure X-Ray diffraction and infrared spectroscopy study. Energy Procedia, v. 37 p. 5892-5896.

Smith, L.B., Leone, J., 2010. Integrated characterization of Utica and Marcellus black shale gas plays, New York State. AAPG Search and Discovery Article, No. 50289, p. 36.

Thommes, M., Cychosz, K.A., 2014. Physical adsorption characterization of nanoporous materials: progress and challenges. Adsorption. v. 20, p. 233-250.

Thommes, M., Cychosz, K.A., 2014. Physical adsorption characterization of nanoporous materials: progress and challenges. Adsorption. v. 20, p. 233-250.

Thommes, M., Kaneko, K., Neimark, A.V., Olivier, J.P., Rodriguez-Reinoso, F., Rouquerol, J., Sing, K.S.W., 2015. Physisorption of gasses, with special reference to the evaluation of surface area and pore size distribution. Pure Appl. Chem. IUPAC Technical Report. p. 19, https://doi.org/10.1515/pac-2014-1117.

Thompson, C.J., Loring, J.S., Rosso, K.M., Wang, Z., 2013. Comparative reactivity study of forsterite and antigorite in wet supercritical CO_2 by in situ infrared spectroscopy. Int. J. Greenhouse Gas Control. v. 18, p. 246-255, http://dx.doi.org/10.1016/j.ijggc.2013.07.007.

US-DOE-NETL, 2015. Carbon Storage Atlas, fifth edition. U.S. Department of Energy—National Energy Technology Laboratory—Office of Fossil Energy.

Wang, Z., Felmy, A.R., Thompson, C.J., Loring, J.S., Joly, A.G., Rosso, K.M., Schaef, H.T., Dixon, D. A., 2013. Near-infrared spectroscopic investigation of water in supercritical CO_2 and the effect of $CaCl_2$. Fluid Phase Equilibria. v. 338, p. 155-163, http://dx.doi.org/10.1016/j.fluid.2012.11.012.

Xamena, F.X.L, Zecchina, A., 2002. FTIR spectroscopy of carbon dioxide adsorbed on sodium-and magnesium-exchanged ETS-10 molecular sieves. Physical Chemistry Chemical Physics, v. 4, p. 1978-1982.

Xue, T., Worthen, A., Qajar, A., Robert, I., Bryant, S.L., Huh, C., Prodanovic, M., Johnston, K.P., 2016. Viscosity and stability of ultra-high internal phase CO_2-in-water foams stabilized with surfactants and nanoparticles with or without polyelectrolytes. Journal of Colloid and Interface Science, v. 461, p. 383-395.

Yang, R., He, S., Yi, J., Hu, Q., 2016. Nano-scale pore structure and fractal dimension of organic-rich Wufeng-Longmaxi shale from Jiaoshiba area, Sichuan Basin: investigations using FE-SEM, gas adsorption and helium pycnometry. Marine and Petroleum Geology, v. 70, p. 27-45, https://doi.org/10.1016/j.marpetgeo.2015.11.019.

Zhang, T., Ellis, G.S., Ruppel, S.C., Milliken, K., Yang, R., 2012. Effect of organic-matter type and thermal maturity on methane adsorption in shale-gas systems. Organic Geochemistry, v. 47, p. 120-131.